PERGAMON

Deep-Sea Research II 49 (2002) 603–621

DEEP-SEA RESEARCH
PART II

www.elsevier.com/locate/dsr2

Quasi-geostrophic 3D circulation and mass transport in the western Bransfield Strait during Austral summer 1995/96

Damià Gomis[a,*], Marc A. García[b,1], Oswaldo López[b], Ananda Pascual[a]

[a] Institut Mediterrani d'Estudis Avançats (CSIC-UIB), Palma de Mallorca, Spain
[b] Laboratori d'Enginyeria Marítima, ETS d'Enginyers de Camins, Canalsi Ports, Universitat Politècnica de Catalunya. Barcelona, Spain

Received 11 May 1999; received in revised form 1 March 2000; accepted 30 May 2001

Abstract

In the framework of the FRUELA carbon-flux study, two oceanographic surveys (December 1995 and January 1996) were conducted by B.I.O. *Hespérides* in the western basin of the Bransfield Strait and southern Drake Passage. The horizontal (geostrophic) velocity field is characterized by two jet-like features linked to frontal hydrographic structures: a meandering current off the continental shelf edge of the southern Drake Passage, corresponding to the Southern front of the Antarctic Circumpolar Current, and the Bransfield Current, related to the Bransfield front. The first jet shows some changes in the meandering pattern from December 1995 to January 1996, whereas the second has a very stationary location and structure. The estimated horizontal circulation and mass transports are compared with available current meter data and with previous geostrophic estimates in the context of a sensitivity analysis that takes into account the choice of the reference level and the station distribution.

The vertical velocity field has been computed by integrating the quasi-geostrophic Omega equation. Maximum estimated values are of the order of 1 m/day, which suggests that a phytoplankton bloom observed in the northern part of the study area in December (and vanished one month later) should not be attributed to frontal dynamic instabilities inducing upward motion and nutricline-related lifting, but rather to other hydrographic factors © 2001 Published by Elsevier Science Ltd.

1. Introduction

A key goal of the FRUELA carbon-flux study was to estimate the 3D mean circulation pattern and the related mass transport contemporary to the acquisition of bio-geo-chemical data, in order to assess further calculations of the carbon advective transport. Results from the US RACER project suggested that the horizontal (advected) flux term in the local carbon budget could be of the order of, or even exceed, the absolute values of respiration (see Table 5 in Huntley et al., 1991), so that precise assessment of the mass transports during the sampled conditions was an obvious need. The purposes of FRUELA in the field of physical oceanography also included estimating the vertical current velocity field in order to assess vertical fluxes.

The companion paper by García et al. (2002) describes the overall hydrographic context of the FRUELA study area and includes a list of relevant

*Corresponding author. Fax: +34-971-173426.
E-mail address: dfsdgb4@ps.uib.es (D. Gomis).
[1] Current address: Direcció General de Portsi Transports, Generalitat de Catalunya, Barcelona, Spain.

PII: S0967-0645(01)00114-X

previous studies on the mean circulation in the Bransfield Strait. In those studies, the mean flow pattern was estimated by computing the geostrophic circulation from hydrographic data alone, with the exception of López et al. (1994) who also used direct current meter measurements. However, none of them included a sensitivity analysis of results or any calculation of vertical velocities.

In this framework, the aim of this work is, first, to estimate the 3D circulation and mass transport associated with main hydrographic structures in the domain covered by the FRUELA field surveys; and, second, to evaluate the sensitivity of results with respect to the reference level used for geostrophic computations and to the station distribution.

2. The data set and data processing

In the absence of direct observations of ocean currents, dynamics has to be inferred from the density field through some balance condition. For some variable (such as the vertical component of the velocity), the balance involves non-linear combinations of high-order spatial derivatives of the density field, then making the reliability of results to be strongly related to the goodness of the data treatment. In the following we describe the data set and data processing leading to all results derived later on, with special attention to the spatial objective analysis. More particular aspects (as the inversion of the Omega equation to estimate vertical velocities) will be described in corresponding sections.

2.1. The data set

The general outlines of the FRUELA cruises and the overall data set have been reported in a companion paper (García et al., 2002). In this work, we will focus on three hydrographic data sub-sets (Fig. 1a):

(i) The macro'95 data set, which consists of 33 CTD profiles distributed along 5 cross-shore

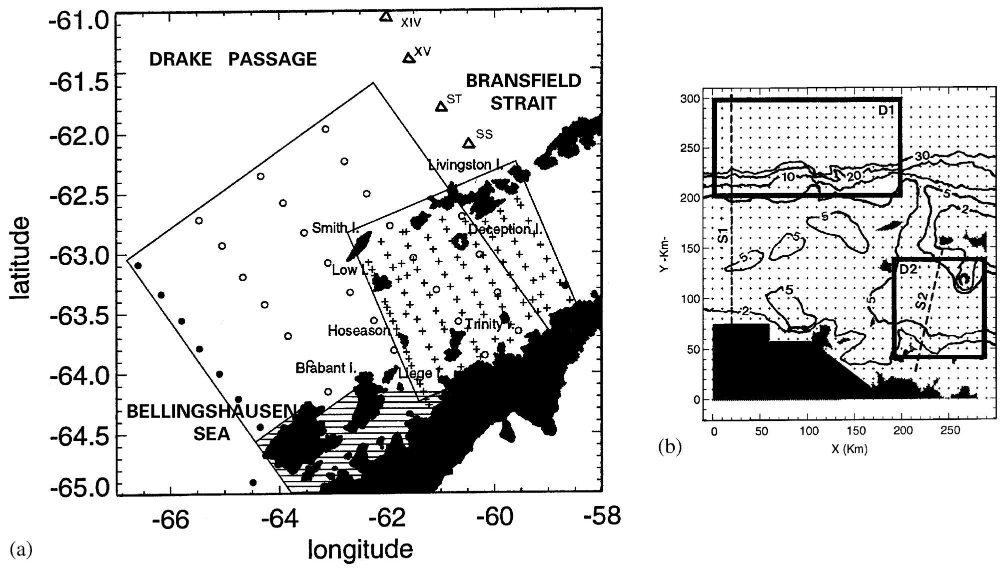

Fig. 1. (a) Location map of the macro'95/96 and meso'95 cruises. Open dots correspond to stations occupied during both the macro'95 and macro'96 cruises, and black dots correspond to stations occupied only during the macro'95 cruise; crosses correspond to the meso'95 cruise. Triangles locate previous current meter deployments. (b) Horizontal grid used for the output of the 2D spatial interpolation in the overall domain, with isobaths in hundreds of meters. Enclosed areas correspond to sub-domains D1, D2 referred in several figures. Dashed straight lines locate vertical cross-sections S1, S2 referred in Figs. 2, 4 and 5.

transects acquired between 3/12/95 and 9/12/95. Along the transects, the separation distance between stations was about 31 km, and the separation between transects was about twice that distance. The sampled domain (roughly $290 \times 290\,\mathrm{km}^2$) covers most of the western basin of the Bransfield Strait, extending westward into the Bellingshausen Sea and northward beyond the continental shelf edge into the southern Drake Passage.

(ii) The meso'95 data set, consisting of 107 CTD profiles obtained between 12/12/95 and 19/12/95 on a regular distribution of stations separated about 14 km. The sampled domain (roughly $170 \times 170\,\mathrm{km}^2$) covers the whole western basin of the Bransfield Strait and partially overlaps with the macro'95 domain (86 of the 107 meso'95 stations fall within the macro'95 domain).

(iii) The macro'96 data set, which consists of CTD profiles acquired on a reoccupation of 27 of the macro'95 stations (all macro'95 stations with the exception of those located on the westernmost transect) between 21/1/96 and 27/1/96.

Comparison of results obtained from the different data sets will be useful to evaluate the sensitivity of the inferred 3D circulation. Firstly, the fact that the macro'95 and macro'96 samplings basically consist of the same stations will allow us to check the circulation changes that occurred in the 40 days that separate both surveys. Secondly, since the macro'95 and meso'95 samplings are very close in time, the overlapping sector between the two will allow a check of the sensitivity of results with respect to the spatial density of the sampling. Finally, the fact that all profiles extend from surface to bottom will allow us to check the sensitivity of results with respect to the reference level chosen for geostrophic computations.

2.2. The spatial objective analysis

In a preliminary step, temperature and salinity raw profiles were used to compute potential density (σ_θ) and specific volume anomaly profiles. The latter were the input data for a principal component (PC) analysis yielding, on output, a set of vertical modes ordered in terms of explained variance. These modes constitute an orthogonal basis in a vector space of dimension equal to the number of levels considered (they are actually referred to as empirical orthogonal functions (EOFs) in the general context of PC analysis), and therefore every profile can be expressed as a linear combination of them. The set of coefficients (or 'amplitudes') corresponding to every vertical mode is a function of the horizontal location of profiles, and can be interpolated from station points onto a regular horizontal grid. Combination of gridpoint amplitudes with the vertical modes results in a 3D discrete representation of the field.

A complete description of the method is given in Pedder and Gomis (1998). Details particular of the present study are summarized in the following. The output grid consisted of 30×30 cells of $10 \times 10\,\mathrm{km}^2$ (see Fig. 1b). For partial analysis of the meso'95 data set we used a 35×35 grid of $5 \times 5\,\mathrm{km}^2$ cells. Amplitudes were interpolated by optimal statistical interpolation (OSI) using a Gaussian correlation model with a 20-km characteristic scale. The standard OSI scheme was convoluted with a normal-error filter (see Pedder, 1993), with a cut-off wavelength set to twice the mean separation distance between stations (80 km for the macro'95 and macro'96 data sets and 30 km for the meso'95 data set).

A major benefit of the PC-based spatial analysis described above is the consistent removal of small horizontal and vertical scales, a crucial feature when derived variables are computed from the 3D density field. A common assumption in spatial objective analysis is that spatial features whose horizontal dimensions are too small to be resolved by the sampling should be filtered out by the interpolation scheme. However, 3D fields often are obtained simply by overlapping a set of horizontally interpolated fields, so that no explicit filtering is applied in the vertical. In our scheme, by examining the lag-correlation between station amplitudes we can determine the vertical modes whose associated horizontal scales can be resolved by the sampling. The crucial feature is that by retaining only the contribution of these modes out of the whole linear combination, both horizontal and vertical small scales are filtered out in a consistent way. In our region, lag-correlation between station pairs was found to be significant only for the first three modes. This meant to consider 96.6% of the total variance as ‘signal’, and the other 3.4% as ‘noise’, the latter including the fraction of variance that, despite not being actual noise, cannot be properly resolved by the station distribution.

A second benefit relevant for geostrophic computations, is the possibility of estimating dynamic height even for profiles not reaching the reference level. More precisely, shallow profiles can be least-square-fitted to the selected modes and the obtained amplitudes used to reconstruct the lower, missing layers of the profiles.

2.3. The reference level

Computation of dynamic height from analyzed specific volume anomaly is straightforward. Concerning the depth of the reference level, it was set to 200 m (the maximum profile depth) in the most complete previous study in this area (by Niiler et al., 1991), and to 500 m in other studies (e.g., Grelowski et al., 1986). Vertical cross-sections of density show that in the northern sector of the surveyed domain (off the continental shelf edge, in the southern Drake Passage) the slope of isopycnals is quite noticeable at 500 m (Fig. 2a). This is due to the presence of a deep frontal structure (Fig. 2b) referred to as the southern boundary of the Antarctic Circumpolar Current (hereafter SbyACC front) by Orsi et al. (1995). Therefore, deep layers are expected to contribute largely to upper geostrophic velocities in this sector.

This is not the case in the other sectors of the surveyed domain. Across the western basin of the Bransfield Strait, for instance, the slope of isopycnals at 500 m is less noticeable and not coherent with upper level density structures (Fig. 2c). A second frontal structure, located over the southern shelf edge of the South Shetland Islands—the so called Bransfield front, is essentially confined to the upper 300 m. Moreover, only small areas of this sector are deeper than 750 m, so that the contribution of deep layers to upper geostrophic velocities is expected to be much smaller. This is even more true further west, over the continental shelf of the Bellingshausen Sea, where the average depth is of the order of 500 m (see Fig. 1b).

It seems, therefore, that 500 m could be a right choice for the reference level except in the northern sector of the domain, where computations shall be referred to a deeper reference level. Setting the reference level to 500 m implies that 15(12) of the 33(27) macro’95(96) profiles are shallower than the reference level. Of these, 3(2) are shallower than 200 m and not intended to be extrapolated downwards. For the meso’95 data set, 40 profiles are shallower than 500 m. Of them, 20 are shallower than 200 m and therefore were discarded for geostrophic computations.

3. Horizontal circulation and mass transport

3.1. Geostrophic velocity field

Geostrophic velocity can be easily derived by finite differencing the dynamic height field. Distributions at 10 and 200 m (Figs. 3a,b for the Macro’95 and Figs. 6a,b for the Macro’96) show the horizontal extension of the two main circulation features referred in the previous section: the meandering jet associated with the SbyACC front, located off the continental shelf edge of the southern Drake Passage, and the Bransfield Current related to the Bransfield front, in the western basin of the Bransfield Strait. The meanders of the first jet apparently break into mesoscale anticyclonic eddies. However, both the scale of these eddies (about the smallest that can be resolved by the sampling) and their location (close to the boundary of the surveyed domain) suggest that one should take their representation with some prevention. On the other hand, the Bransfield jet exhibits a well-defined cyclonic circulation extending over most of the western basin of the Bransfield Strait. The hydrographic characteristics of both frontal structures have been discussed by García et al. (2002).

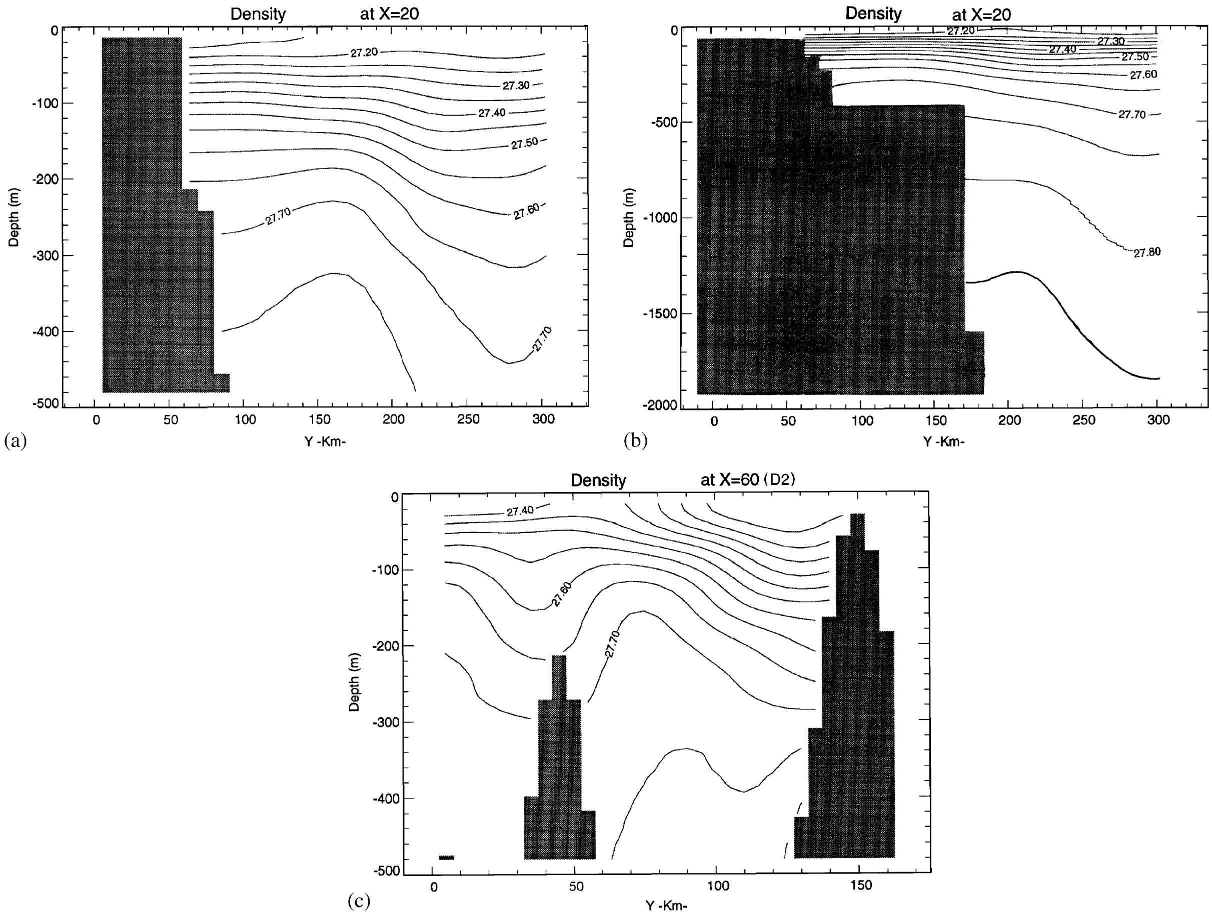

Fig. 2. Potential density (σ_θ) computed from the macro'95 data set: (a) on vertical section S1 (located in Fig. 1b); (b) as in (a), but extending to 2000 m; (c) as in (a), but for vertical section S2.

Comparison of Fig. 3a with b (or Fig. 6a with b) reveals that the main structures exhibit a very similar shape at different depths. This keeps true at all depths down to the reference level and is a consequence of the almost total absence of vertical tilting of density structures observed over most of the domain. The only exception is the cyclonic structure in the western basin of the Bransfield Strait, which is very apparent at surface but weaker at 200 m. This makes the Bransfield Current better defined at 200 m, as it flows along the southern shelf edge of the South Shetland Islands. A better picture of this area obtained from the full resolution meso'95 data set will be shown later in this section.

Comparison of Figs. 3a,b with 6a,b reveals some changes in the shape of the SbyACC jet between December 1995 and January 1996. In principle it is difficult to state whether the meander of Fig. 6 is the same as the collocated meander of Fig. 3 (in which case the western meander of Fig. 3 would have decayed) or, instead, both meanders have been advected downstream, so that the meander observed in Fig. 6 is the same as the western meander of Fig. 3. The slight vertical tilting observed in this region is more consistent with the second hypothesis, since for neutral modes vorticity structures can only be advected, not reinforced or decayed. The Bransfield Current exhibits a very stationary location and structure.

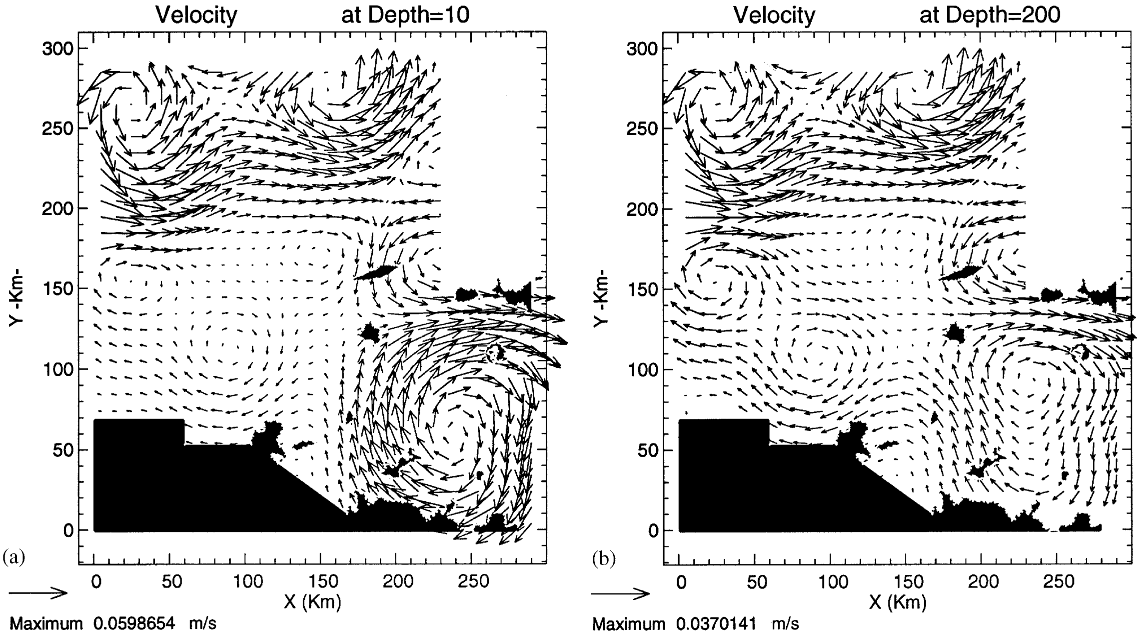

Fig. 3. Geostrophic velocities (referred to 500 m) computed from the macro'95 data set at: (a) 10 m; (b) 200 m.

This is also the case for most minor eddy structures, although they appear more reinforced in Fig. 6 (late January) than in Fig. 3 (early December).

To provide support for the sensitivity tests presented in the appendix, geostrophic velocities were recomputed in a different way in two sub-domains: in the northern sector (sub-domain D1, Fig. 1b) they were estimated from the same (macro'95) data set, but referred to 2000 m (Fig. 4); in the western basin of the Bransfield Strait they were computed with respect to the same reference level (500 m), but from the high-resolution meso'95 data set (Fig. 5). Comparison of Figs. 3a and 4a shows that when referred to 2000 m the SbyACC jet is almost three times stronger than when referred to 500 m (maximum values at 10 m are about 17 and 6 cm/s, respectively). The vertical structure of the jet (Fig. 4b) confirms that geostrophic velocities are significant over the whole vertical extension of the domain. In particular, at 500 m they are about 10 cm/s at the jet core (increasing up to 14 cm/s further east). Very similar results were obtained for the macro'96 data set (not shown).

In the Bransfield Strait, the analysis of the meso'95 data set (Fig. 5a) uncovers the details of the overall cyclonic circulation shown in Fig. 3a. It shows, for instance, that water of Weddell influence flowing southwestwards along the Antarctic Peninsula continental shelf breaks into well-defined mesoscale cyclonic eddies as it recirculates within the western basin of the Bransfield Strait. In the western sector of the basin the southwestwards flow joins a weaker northwesterly flow from the Drake Passage, resulting in a reinforced northeastwards current (the Bransfield Current) that is clearly defined as it flows along the southern shelf edge of the South Shetland Islands. Maximum surface values of about 16 cm/s are obtained as the Bransfield jet approaches the eastern boundary of the domain. A vertical section across the basin (Fig. 5b) shows the Bransfield Current located over the shelf edge, as well as the southwestwards inflow located to the north of Trinity Island. According to the density distribution (Fig. 2c), significant geostrophic velocities are essentially confined to upper levels (at 300 m, maximum

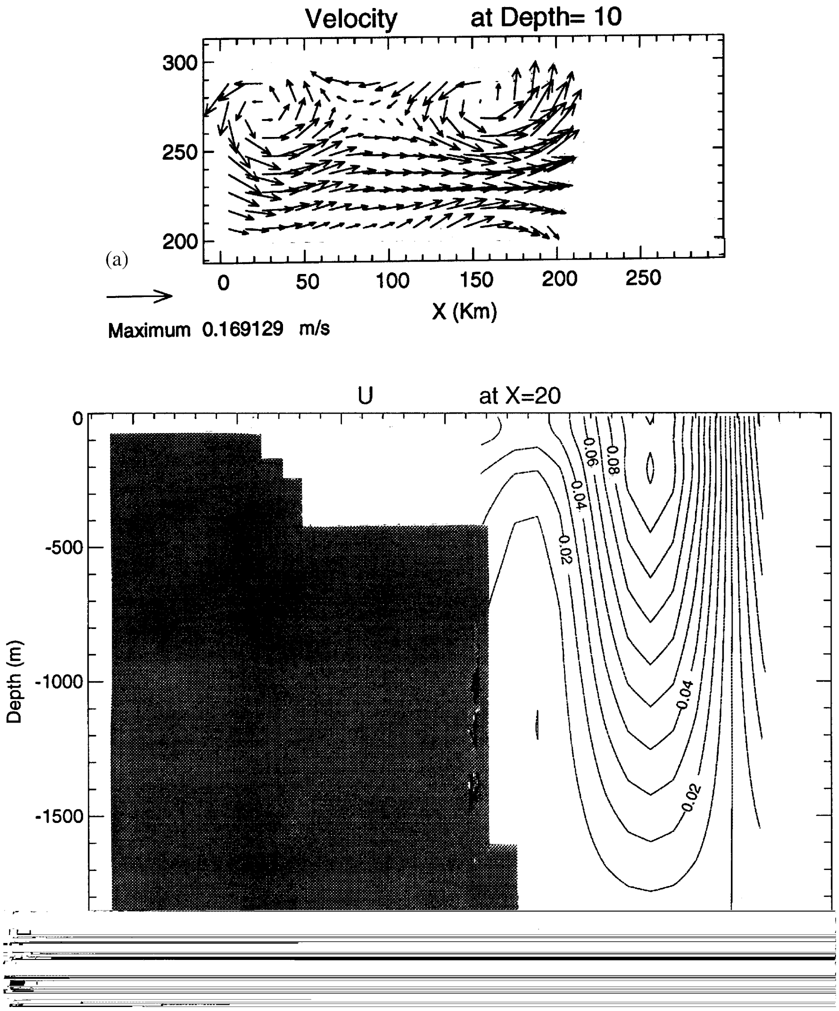

Fig. 4. Geostrophic velocities (referred to 2000 m) computed from the macro'95 data set in sub-domain D1 (Fig. 1b): (a) distribution at 10 m; (b) across vertical section S1 located in Fig. 1b (in m/s, with the usual sign convention).

values corresponding to the Bransfield jet core are <3 cm/s).

3.2. Comparison with previous in situ measurements

To our knowledge, the only current meter data acquired on the stretch of the northern South Shetland continental slope are the one-year records obtained in the framework of the ISOS' DRAKE 75 and DRAKE 79 experiments. In particular, moorings "XIV" and "XV" of DRAKE 75 were deployed north of Livingston Island, off the continental shelf edge (approximately on 61°00′S, 62°00′W and 61°24′S, 61°42′W, respectively, at 3750 m water depth) and had single RCM current meters at 2667 and 2744 m, respectively. On the other hand, moorings "ST" and "SS" of DRAKE 79 also were deployed north of Livingston Island, but over the continental slope (the first on 61°48′S, 61°08′W at 3070 m water depth, and the second on 62° 05′S, 60°35′W at 600 m) with RCM current meters at 680, 1400 and 2710 m depths (for "ST") and at 500 m depth (for "SS"). All these moorings are close to

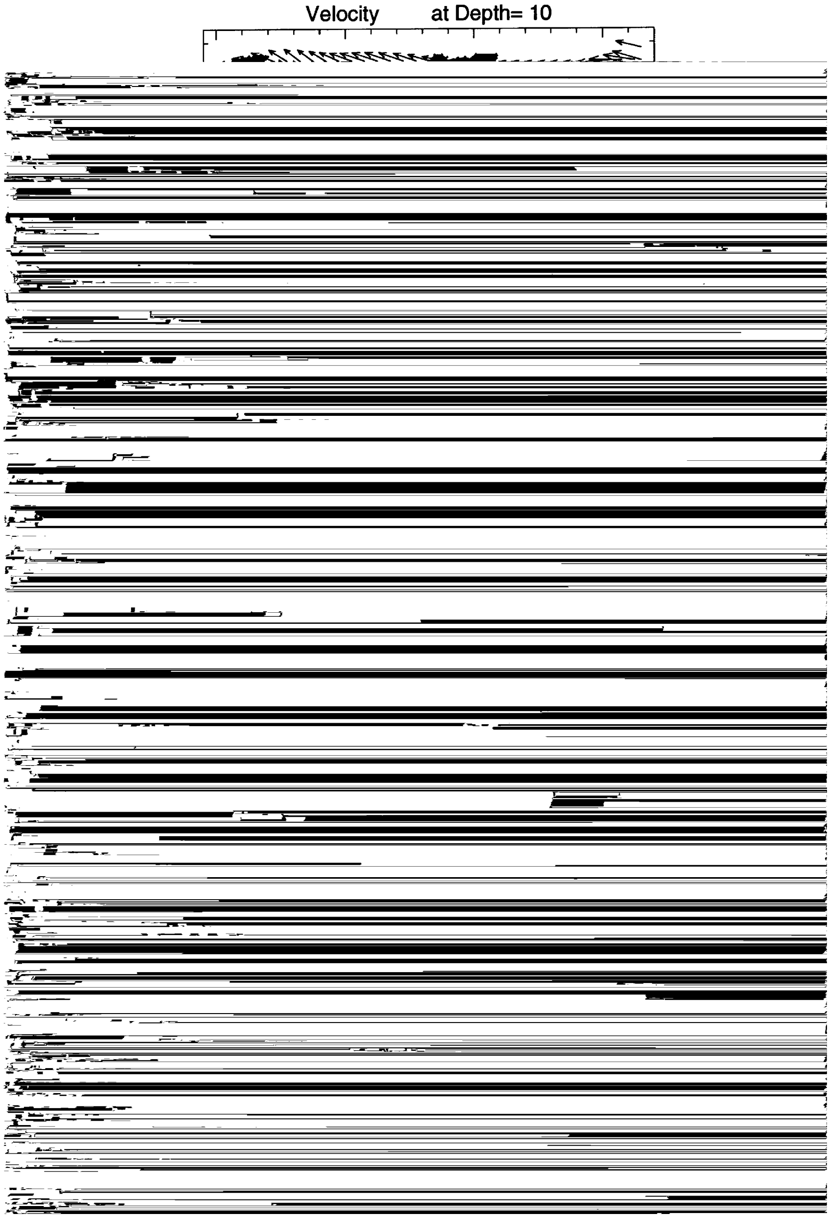

Fig. 5. Geostrophic velocities (referred to 500 m) computed from the meso'95 data set (sub-domain D2 in Fig. 1b): (a) distribution at 10 m; (b) across vertical section S2 located in Fig. 1b (in m/s, with the usual sign convention).

(though out of) the FRUELA study domain (see Fig. 1a).

For the outer current meters, Nowlin et al. (1977) reported yearly averaged cross-section speeds (towards 62°) of 4.9 cm/s (for "XIV") and 2.1 cm/s (for "XV"). Bryden and Pillsbury (1977) focused on the time variability of current records, reporting weekly averaged values ranging between −3.5 and 11.5 cm/s (with a standard deviation of about 3 cm/s) for current meter "XIV". For the arrays located on the continental slope, Nowlin and Zenk (1988) computed a long-term averaged flow of 8.6 cm/s towards 259° (following the isobaths in a westwards direction) for the "ST-2710" current meter, and of the order of 1 cm/s for "ST-1400". For the shallower "SS-500" current meter, the reported mean velocity is 5.1 cm/s towards 240° (roughly the same direction as for the "ST" array). Current measurements acquired off the shelf edge ("XIV" and "XV" in Fig. 1) are slightly displaced offshore with respect to the core of the SbyACC jet (Fig. 3). Considering the values reported by Nowlin et al. (1977) as representative of the SbyACC frontal current could suggest that geostrophic computations referred to 2000 m would underestimate actual velocities (both actual velocities measured at 2700 m and upper-level geostrophic velocities are roughly in the same direction). However, the results obtained by Nowlin and Zenk (1988) indicate that this is not the case. They show the presence of a westwards near-bottom current flowing along the continental slope, below the onshore side of the SbyACC jet. That current originates in the Weddell Sea and it was not observed by the many earlier ISOS observations in the Drake Passage because those measurements were not made close enough to the bottom along the southern slope. According to Nowlin and Zenk (1988), a narrow tongue of that current underlying the SbyACC front extends as far as 65°W (this is, all along the stretch of the continental shelf edge covered by the FRUELA study domain). Although it is difficult to be precise using Nowlin and Zenk's (1988) figures, the turning point between the upper-layer northeasterly flow and the westwards deep flow would be slightly deeper than 2000 m over the greatest depths of the continental slope. This would confirm that the reference level used for geostrophic computations in the northern sector of our domain is basically correct.

The near-bottom current detected over the greatest depth of the shelf edge extends to the whole water column over the shallower parts of the edge and over the continental shelf of the South Shetland Islands (Whitworth III et al., 1982). Within our domain, the westernmost upper-level signature of that westwards current can be seen in the geostrophic velocity distributions of Fig. 3, as inferred from dynamic height referred to 500 m computed at stations located to the north of Smith Island. It can also be figured out (though less clearly) in Fig. 6, from the deflection and reversal trend of the northeastwards current observed to the northwest of Smith Island.

For the Bransfield jet, direct current measurements obtained south of Deception Island during Austral summer 92/93 were processed by López et al. (1994), who reported maximum current speeds between 17 and 20 cm/s for the mean flow (after filtering out the tidal variability). The ancillary geostrophic computations show that their mooring "2" was deployed right on the core of the Bransfield Current. The fact that measured current speeds are only slightly larger than the 16 cm/s obtained from geostrophic computations provide evidence for the appropriateness of the reference level choice in this sector.

3.3. Transport across relevant sections

Transports have been computed across different sections of the domain (Fig. 7a). Sections S1, S2, and S3 provide a measure of the transport associated with the SbyACC front, for which geostrophic velocities have been referred to 2000 m. Transports across S4, S5, and S6 measure the exchanges between the western basin of the Bransfield Strait and adjacent basins, and have been computed from the high resolution meso'95 data set (with reference level at 500 m). The background field of Fig. 7a is only intended to locate the sections with respect to the overall circulation pattern in the domain, but none of the transports can be strictly related to the stream lines shown in this Figure. Sections S1, S2 and S3 should actually be related to dynamic height lines referred to 2000 m (inferred from Fig. 4a), whereas sections S4, S5 and S6 should be related to dynamic height lines computed from the meso'95 data set (inferred from Fig. 5a).

Section S1 intends to evaluate the flow (from surface to 2000 m) through the western boundary

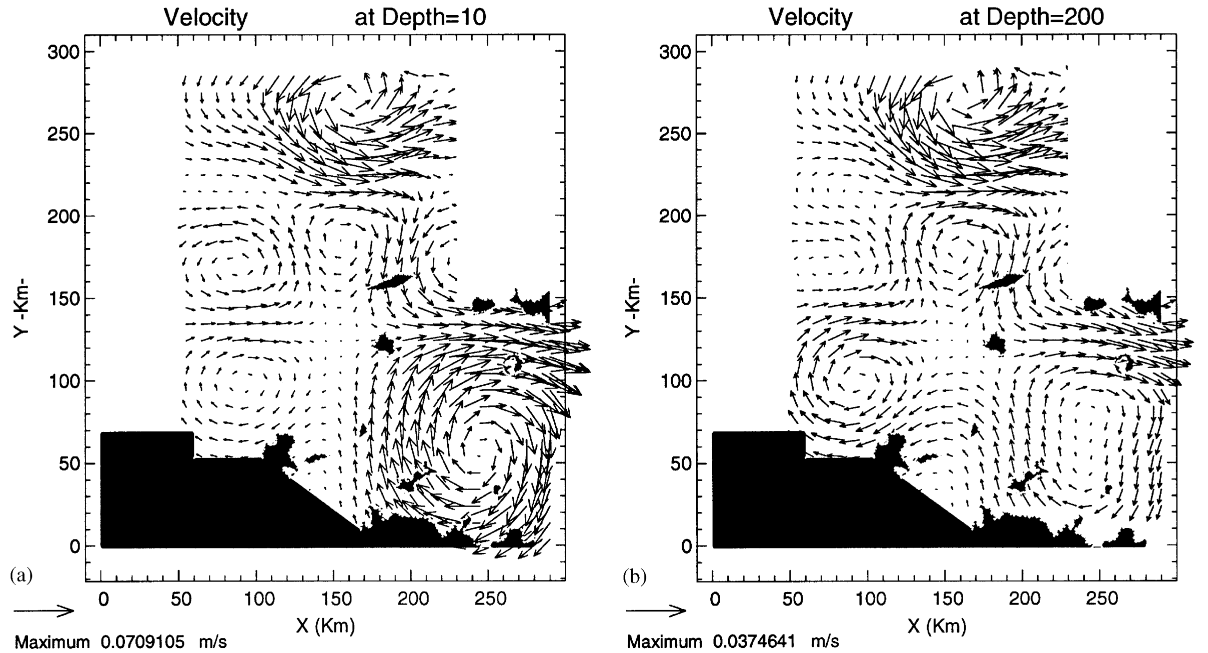

Fig. 6. Geostrophic velocities (referred to 500 m) computed from the macro'96 data set at: (a) 10 m; (b) 200 m.

of the sampled domain (about 6 Sv). The difference of about 2 Sv with respect to S2, located downstream, can be attributed to differences in the recirculation within the jet meanders (maximum speeds are observed associated with the eastern meander). Section S3 intends to evaluate the flow through the northern boundary of the sampled domain (about 5 Sv). Transports computed from the macro'96 horizontal velocities (Fig. 6a) were quite similar. Because the SbyACC front may not be completely covered within the sampled domain, the values given in Fig. 7b must be taken only as a first guess of the associated transport. On one hand, transports computed for sections extending beyond the northern boundary of our domain are obviously expected to be larger. On the other hand, part of the estimated transports (specially across S1 and S2) might recirculate within the meandering structure of the jet, so that the net northeastward transport could also be smaller. In any case, our values are by far larger than the 0.5–0.6 Sv given by Grelowski et al. (1986), who derived geostrophic velocities from dynamic height referred to 500 m computed on a coarser station distribution.

Section S4 (Fig. 7c) intends to measure the exchanges between the Bransfield Strait and the Bellingshausen Sea through the channels between Smith, Low, Hoseason and Trinity Islands. Results show exchanges in both senses, with a

Fig. 7. (a) Location of vertical sections referred in (b)–(e); background field is dynamic height (in dyn m) at 10 m (referred to 500 m) computed from the macro'95 data set. (b) Net eastward transport (between surface and every depth) across sections S1 (80 km) and S2 (70 km) and net northward transport across section S3 (90 km), computed from the macro'95 data set with geostrophic velocities referred to 2000 m. (c) Positive (eastward), negative (westward) and net transport across section S4 (120 km), computed from the meso'95 data set with geostrophic velocities referred to 500 m. (d) As in (c), but for section S5 (50 km), taking positive (negative) transport northward (southward). (e) As in (c), but for section S6 (50 km).

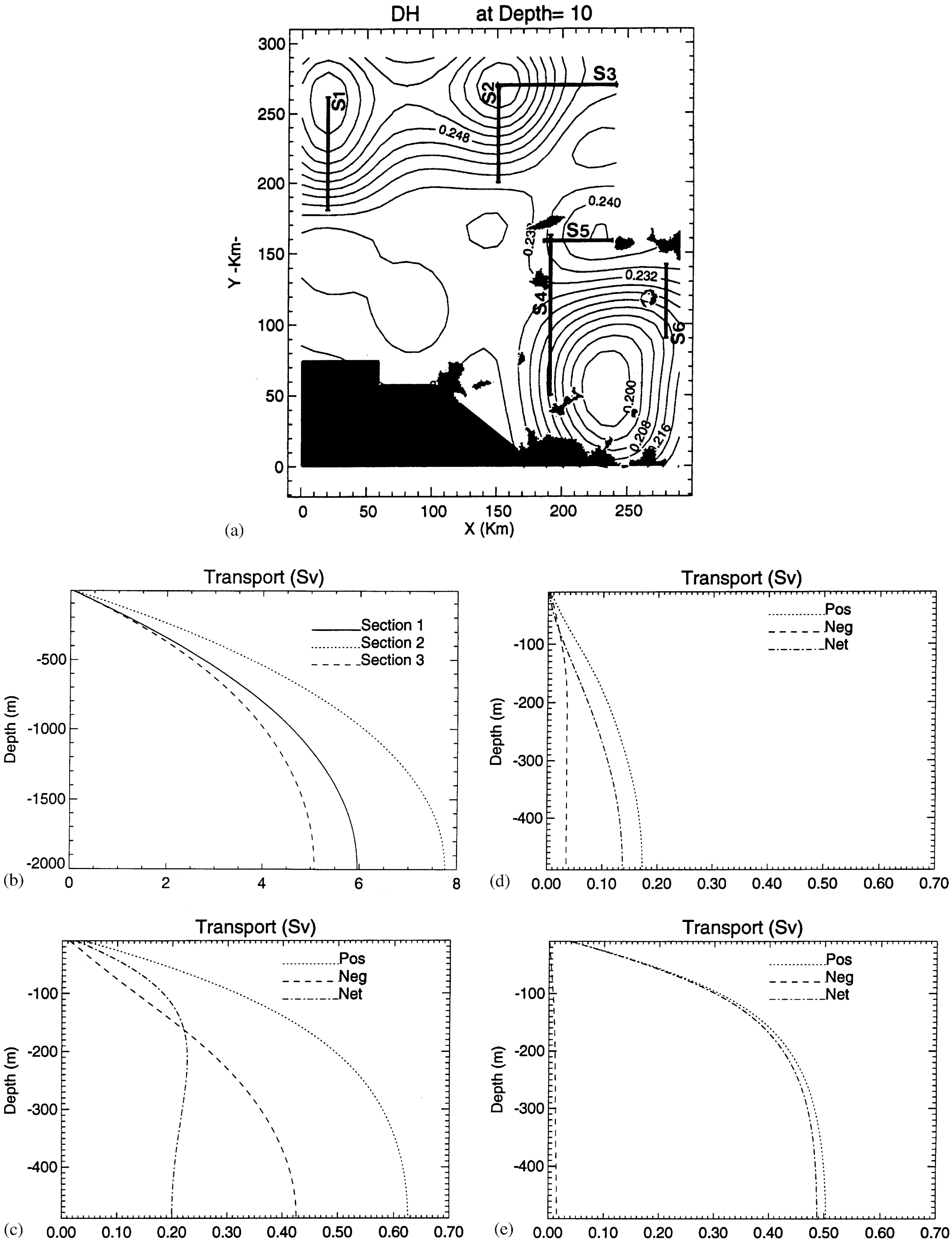
DH at Depth= 10
Y -Km-
X (Km)
S1
S2
S3
S4
S5
S6
0.248
0.240
0.232
0.200
0.208
0.216
(a)
Transport (Sv)
Depth (m)
Section 1
Section 2
Section 3
(b)
Transport (Sv)
Depth (m)
Pos
Neg
Net
(c)
(d)
(e)

net entrance into the Bransfield Strait of about 0.2 Sv (from surface to 500 m). A smaller amount of water (about 0.14 Sv) seems to exit the Bransfield Strait northwards, across section S5 (Fig. 7d). It is worth noting that the background field of Fig. 7a (or, equivalently, of Figs. 3a,b) indicates a southward net flux across S5, which gives an idea of the sensitivity of transport estimates with respect to the station distribution. Nevertheless, the net northward transport obtained across S5 does not imply that the Bransfield Strait is exporting water towards the Drake Passage. Instead, the westward current observed over the northern shelf of the South Shetland Islands seems to recirculate anticyclonically, joining a north-westerly flow and re-entering the Bransfield Strait across the western channels (see Figs. 3a and 5a).

Finally, section S6 (Fig. 7e) accounts for the transport of the Bransfield Current at the eastern boundary of the domain. The obtained value of 0.5 Sv is in fairly good agreement with Grelowski et al. (1986) and is obviously larger than the values given by Niiler et al. (1991), who referred geostrophic velocities to 200 m. Grelowski et al. (1986) and López et al. (1999) also measured the transport of the Bransfield Current in the central and eastern basins of the Bransfield Strait, respectively. Both report maximum transports of about 1 Sv over the sill separating the central and eastern basins. This implies that the recirculation of water of Weddell origin that reinforces the Bransfield Current in the western basin (Fig. 5a) also should take place farther east (in the central basin).

4. Vertical velocity field

4.1. Computation of vertical velocities

The relationship between the horizontal and vertical velocity (w) components can be derived from the quasi-geostrophic (QG) vorticity and thermodynamic equations (Holton, 1979). Eliminating the time derivatives between the two and assuming that w varies with depth much more rapidly than density yields a diagnostic equation known as the Omega equation:

$$\left(N^2\nabla_{\mathrm{h}}^2 + f_0^2\frac{\partial^2}{\partial z^2}\right)w = f_0\frac{\partial}{\partial z}[\vec{V}_{\mathrm{g}}\cdot\nabla(f+\zeta_{\mathrm{g}})] + \frac{g}{\rho_0}\nabla_{\mathrm{h}}^2[\vec{V}_{\mathrm{g}}\cdot\nabla\rho], \tag{1}$$

where N is the Brunt-Väisälä frequency, ∇_{h} is the horizontal gradient operator, $\vec{V}_{\mathrm{g}}$ is the geostrophic velocity, ζ_{g} is the geostrophic relative vorticity and other symbols have conventional meanings. As shown in (1), the QG vertical forcing depends on the vertical derivative of vorticity advection by the geostrophic current and on the horizontal Laplacian of density advection.

A drawback of the Omega equation is that the two terms on the right-hand side can approximately cancel each other when dynamics is dominated by baroclinic instability (Hoskins et al., 1978). This is not the case for the fields we are dealing with, for which the first term on the right-hand side of (1) dominates over the second due to the practical absence of vertical tilting over most of the domain (for purely neutral modes the second term would be zero). Nevertheless, we used the QG Omega equation re-written in the form introduced by Hoskins et al. (1978), which overcomes the cancellation problem

$$\left(N^2\nabla_{\mathrm{h}}^2 + f_0^2\frac{\partial^2}{\partial z^2}\right)w = 2\nabla_{\mathrm{h}}\cdot\vec{Q}, \tag{2}$$

where

$$\vec{Q} = \frac{g}{\rho_0}\left(\frac{\partial\vec{V}_{\mathrm{g}}}{\partial x}\cdot\nabla_{\mathrm{h}}\rho, \frac{\partial\vec{V}_{\mathrm{g}}}{\partial y}\cdot\nabla_{\mathrm{h}}\rho\right). \tag{3}$$

Eq. (2) (also (1)) is a Poisson type equation that can be solved in a 3D domain provided that boundary conditions are specified. These can reasonably be set to zero at the bottom and at surface, but lateral boundary conditions are more arbitrary. Nevertheless, the sensitivity of vertical velocity fields to lateral boundary conditions usually restricts to the few outermost rows and columns of the 3D grid, with no influence on the results obtained in the inner domain. This was checked to be true in our case, and therefore lateral boundary conditions also were set to zero for simplicity.

From the 3D vertical velocity field obtained after numerical integration we show the distributions at 100 m (Figs. 8a and 9), the level around which maximum values were obtained. Both the macro'95 and macro'96 distributions essentially show small scale structures mainly associated with

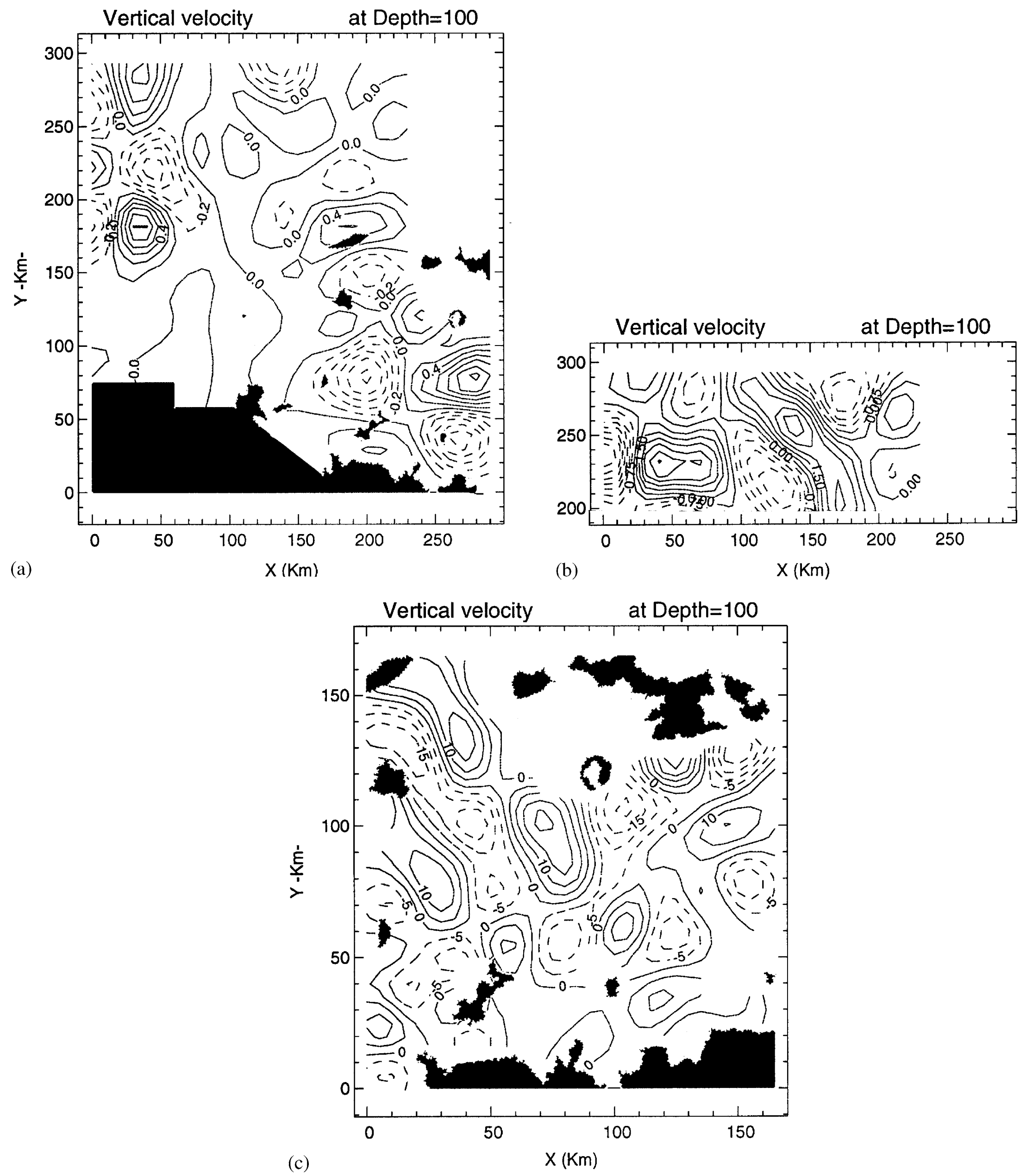

Fig. 8. Vertical velocity (in 10^{-6} m/s) at 100 m computed from: (a) from the macro'95 data set, with reference level at 500 m; (b) the macro'95 data set, with reference level at 2000 m (sub-domain D1 in Fig. 1b); (c) the meso'95 data set (sub-domain D2 in Fig. 1b), with reference level at 500 m.

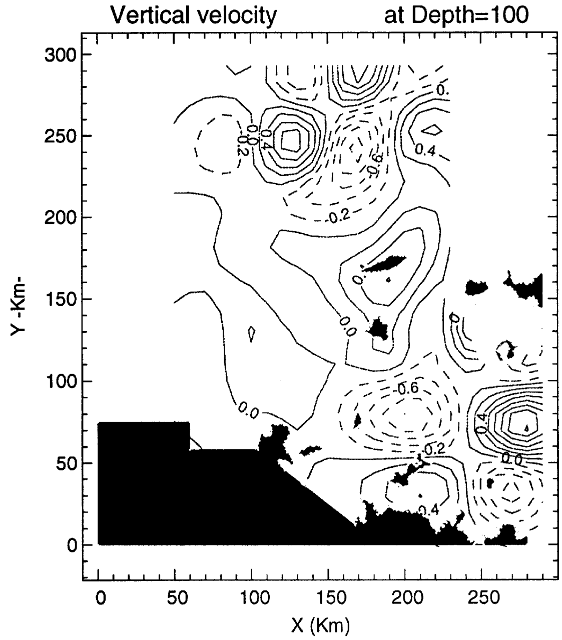

Fig. 9. Vertical velocity (in 10^{-6} m/s) at 100 m (reference level at 500 m) computed from the macro'96 data set.

the two main jets. The absence of predominant features is consistent with the very low values (<10 cm/day) obtained in our domain. [In frontal regions, vertical velocities can be of the order of 10–90 m/day (see for instance, Pinot et al., 1996). Nevertheless, the vertical velocity pattern associated with the Bransfield jet in December 1995 and January 1996 (Figs. 8a and 9) is very similar, which confirms the high degree of stationarity of the jet. This is obviously not the case for the SbyACC jet, for which geostrophic velocity patterns in December and January were rather different.

In order to check the sensitivity of these values, (2) was also integrated for sub-domain D1 of Fig. 1b, referring dynamic height to 2000 m (Fig. 8b), and for the full resolution meso'95 data set, keeping the reference level at 500 m (Fig. 8c). In the first case the values obtained increase up to 0.5 m/day, and in the second case they reach 1.5 m/day at the cores of ascent and descent structures.

4.2. 3D circulation and bio-geo-chemical implications

It is well known that frontal currents can induce strong upward motions, which result in the fertilization of the euphotic layers and, therefore, in primary production. However, this does not seem to be the case that derives from previous results. Upward velocities of 1 m/day would require of the order of 50 days to yield meaningful ascents, which is about three times the time required for a water parcel to be horizontally advected through the whole domain. In another way, a water parcel would take about 5 days to cross ascent/descent features of the order of 50 km, such as those seen in Figs. 8 and 9. In that time, resulting vertical displacements would be less than 5 m (assuming that the advection of the ascent/descent pattern by the mean flow is much slower than the flow speed).

Figs. 10a,b show the fluorescence distribution as given by the CTD probe for the macro'95 and macro'96 data sets. The differences between the two are very obvious: in early December 1995 a high concentration of pigments was observed related to the SbyACC frontal region (and, to a much lesser extent, within the Bransfield Strait), whereas no significant concentrations were observed on late January 1996. These features are interpreted as the result of a late spring phytoplankton bloom which was no longer active in January (Castro et al., 2002). This interpretation is supported by the contemporary surface horizontal distributions of dissolved oxygen, nitrates and total inorganic carbon reported by García et al. (2002).

At first it was thought that the observed seasonal difference could be attributed to changes in the dynamics (e.g., in the induced upward/downward motion) of the meandering SbyACC current. However, as seen in the previous section, the magnitude of vertical velocities does not differ substantially from December to January (Figs. 9a and 10), and in any case it is too small to produce a significant ascent of nutrients. Therefore, the bloom observed during the late spring survey should not be attributed to local frontal dynamic instabilities generating upward motion. Instead, it

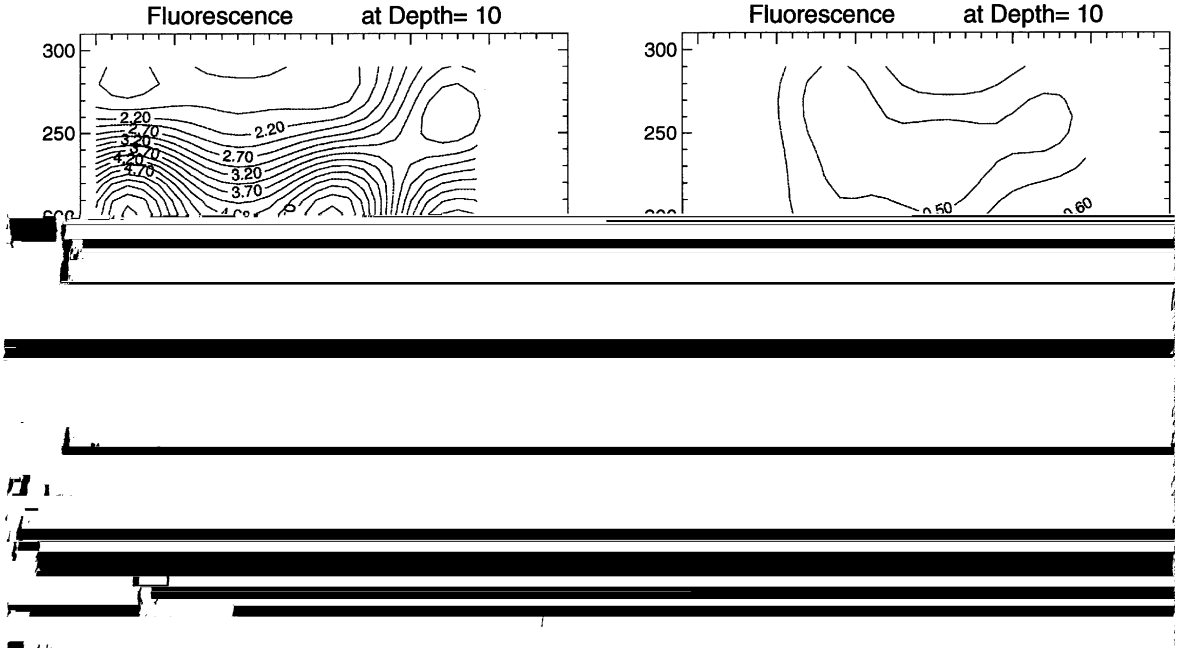

Fig. 10. Fluorescence distribution (arbritrary units) at 10 m for: (a) the macro'95 data set; (b) the macro'96 data set.

should either be produced in a different region and reach our domain advected by the mean flow, or be produced locally in relationship to transient stability conditions in the water column linked to the influence of sea ice melting in late spring.

5. Discussion and conclusions

Because the horizontal (advected) flux term plays a key role in the local carbon budget, assessing the accuracy of transport estimates is almost as important as the transport values. In Appendices A and B we evaluate the sensitivity of inferred geostrophic velocities with respect to the reference level and to the station distribution. In the following, some of the estimates given in Section 4 will be discussed in the light of these sensitivity tests and main conclusions will be outlined.

In the northern sector of the domain, off the shelf edge of the southern Drake Passage, 2000 m seems to be an acceptable choice for the geostrophic reference level. Instead, the coarse station distribution of the macro'95 and macro'96 surveys is likely to produce some underestimation of geostrophic velocities due to the compulsory smoothing of dynamic height analysis. Qualitative comparison with the underestimation observed in the Bransfield Strait suggests that geostrophic velocities could exceed 20 cm/s, which would be in good agreement with velocity measurements reported by Nowlin and Zenk (1988). Nevertheless, part of the velocity variance not captured by the analysis is expected to be associated with transient mesoscale features and therefore not contribute to the mean flow transport. The circulation pattern is less sensible to the sampling problem and it is expected to be essentially correct, as well as the circulation changes observed from early December 1995 to late January 1996.

In the Bransfield Strait, our previous estimates are expected to be more accurate. Firstly, because the station distribution is optimal for the recovering of mesoscale geostrophic features, and secondly, because the eventual underestimation derived from the reference level is also small. Moreover, our estimates were shown to be consistent with direct current meter measurements in this sector. Our values are also in agreement with those given by Grelowski et al. (1986), who evaluated the geostrophic current referred to 500 m at different cross-sections and reported maximum values ranging from 7 to 26 cm/s. On the other hand, Niiler et al. (1991) obtained maximum values (referred to 200 m) between 5 and 8 cm/s, from a station network denser than the macro'95 sampling but sparser than the meso'95 sampling. Their values are consistent with the underestimation predicted by our sensitivity test, which shows that at 10 m, the mean speed referred to 200 m and computed from a low-resolution sampling is 2.25 cm/s, whereas it increases up to 6 cm/s when referred to 500 m and computed from the full resolution meso'95 sampling (Fig. 13).

Concerning the vertical component of the velocity field, a main result is that maximum values obtained by integration of the QG Omega equation are of the order of 1 m/day. This suggests that a phytoplankton bloom observed in the northern part of the study area in December 1995 (and vanished one month later) should not be attributed to frontal dynamic instabilities inducing upward motion and nutricline-related lifting, but rather to other hydrographic factors. Another feature worth noting is the very small seasonal variability observed for the Bransfield front, to the point that even vertical velocity structures associated with the jet are very similar in early December 1995 and in late January 1996.

Acknowledgements

We wish to express our deepest gratitude to J. Figa, M. Gonzàlez, J. Puigdefàbregas, P. Rojas, M. Farran, J. Guillén and P. Masqué for their collaboration in the data acquisition, and to Drs. M. Estrada and R. Anadón, scientific chiefs of the FRUELA 95 and FRUELA 96 cruises. We also want to thank the technical staff and crew of the B.I.O. *Hespérides* for their help and support. This study has been funded by the Spanish Comisión Interministerial de Ciencia y Tecnología under contract ANT94-1010.

Appendix A. Sensitivity of geostrophic computations to the reference level

The problem of the reference level is particularly relevant to horizontal transports, since velocity differences of a few cm/s extending over the whole vertical domain result in substantial transport differences. In order to evaluate the sensitivity of previous results, we computed the mean surface (10 m) speed as a function of the reference level depth for sub-domains D1 and D2 (Fig. 1b). In sub-domain D1, the mean surface geostrophic speed referred to 500 m is about 3 cm/s, whereas it is about 8 cm/s when referred to 2000 m (Fig. 11). This implies, for instance, that the mean transport across a vertical section 50 km wide and 500 m deep would be of the order of 0.37 Sv when using 500 m as reference level, and about 1.75 Sv using 2000 m as reference level. The total transport for a section 2000 m deep would be about 4 Sv.

Fig. 11 also shows that the increasing rate of the mean surface speed with respect to the reference depth (the curve slope) is very pronounced at 500 m: about 0.60 (cm/s)/100 m. At 2000 m it is slightly smaller, but still significant: about 0.32 (cm/s)/100 m. However, the slope is expected to decrease and reverse from then on, due to the presence of the westwards deep current reported by Nowlin and Zenk (1988) (at least for the region closer to the shelf edge). Hence, we will assume

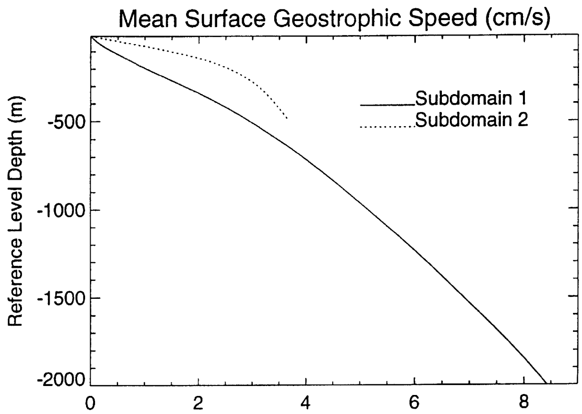

Fig. 11. Mean surface geostrophic speed as a function of the reference level depth computed for sub-domains D1, D2 (Fig. 1b).

that 2000 m (about the turning depth) is a reasonable reference level to compute the transport associated with the SbyACC frontal current. Concerning the transport associated with the westward bottom current, Nowlin and Zenk (1988) report values between 1.4 and 3.2 Sv, which should therefore be subtracted to the SbyACC transport in order to obtain surface-to-bottom net transports. The fact that in our domain only a few stations are significantly deeper than 2000 m prevents from recomputing geostrophic shears relative to a deeper reference level in order to check Nowlin and Zenk's (1988) estimate.

For sub-domain D2, in the western basin of the Bransfield Strait, the mean surface geostrophic speed was not referred to levels below 500 m in order to avoid most profiles not reaching the reference level. Results show that at 500 m the increasing rate of the mean surface speed with respect to the reference depth is significantly smaller than for sub-domain D1 (Fig. 11): 0.25 (cm/s)/100 m. In the worst case of keeping this trend with depth, the mean surface geostrophic speed referred to 750 m (the deepest reasonable depth to which it could be referred) would be about 4.27 cm/s, in front of the 3.65 cm/s obtained when it is referred to 500 m. In terms of transport, this means ranging from 0.45 to 0.71 Sv for a 50 km wide and 500 m deep section (the total mean transport across a 750 m deep section would be 0.8 Sv).

It must be pointed out that in the western basin of the Bransfield Strait only a small sector is as deep as 750 m, so that the eventual underestimation resulting from using 500 m as reference level would only apply to that sector (the overall underestimation would be substantially lower). On the other hand, choosing 250 m as reference level would lead to mean transports of the order of 0.18 Sv (across a 50 km wide and 250 m deep section), which gives an idea of the underestimation of transports evaluated by Niiler et al. (1991).

Appendix B. Sensitivity of geostrophic computations to the station distribution

The smoothing of the spatial objective analysis is aimed to filter out those scales that cannot be resolved by the sampling and, therefore, it is related to the mean separation distance between stations. As pointed out in Section 2, the cut-off wavelengths were set to 80 km for the macro'95 and macro'96 data sets and to 30 km for the meso'95 data set. When applied to dynamic height fields, the degree of smoothing obviously influences subsequent geostrophic velocity computations. It must be stressed that this influence is neither an analysis artefact nor an analysis limitation. It is simply the consequence of the different spectral contents included in the analyzed fields, which are imposed by the station separation.

In order to evaluate the dependence of geostrophic velocities with respect to the station separation, we used the meso'95 data set in two different ways: (i) with the full station resolution, and (ii) using a subset of stations (one out of eight) resulting in a mean separation distance similar to the macro'95 and macro'96 data sets. Surface dynamic height analysis computed from the two data sets are shown in Fig. 12. Fig. 12b shows an overall cyclonic circulation similar to that obtained in this sector from the macro'95 data set (Figs. 3a and 7a). Instead, the full resolution analysis (Fig. 12a) is able to capture mesoscale structures that are absent from the low-resolution analysis. In particular, the height gradients across the Bransfield Front appear more confined and substantially sharper: 4.5 dyn cm over 30 km in Fig. 12a in front of 3.5 dyn cm in Fig. 12b. The mean geostrophic speed referred to 500 m has been computed at every level for both cases (Fig. 13). It reveals that, on average, geostrophic speeds computed from the low resolution sampling are about 40% smaller than those obtained from the full-resolution sampling.

An obvious question is whether geostrophic speeds would continuously increase by decreasing the station separation. Our guess is that computed speeds might certainly increase, but on the other hand, applying the geostrophic assumption to spatial scales smaller than those of Fig. 12a could be questioned. Taking $L = 7.5$ km (the radius of the smallest eddy resolved by the meso'95 data set) and $U = 10$ cm/s, gives a value of 0.1 for the Rossby number. Decreasing the station separation

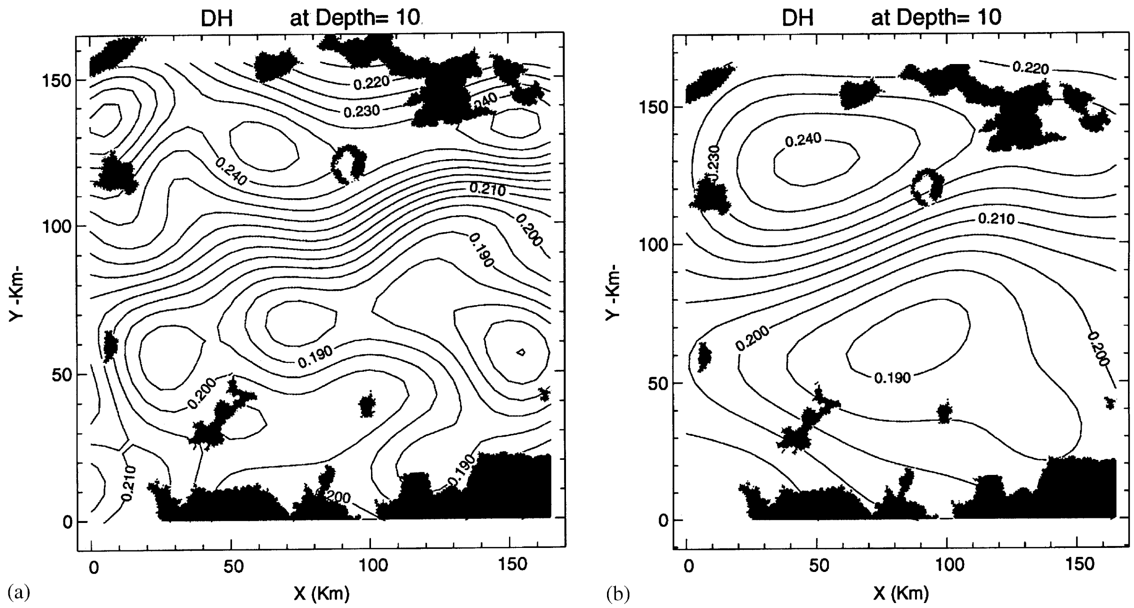

Fig. 12. Dynamic height (in dyn m) at 10 m (referred to 500 m) computed in sub-domain D2 (Fig. 1b) from: (a) the whole meso'95 data set; (b) a subset (one out of eight stations) of the meso'95 data set.

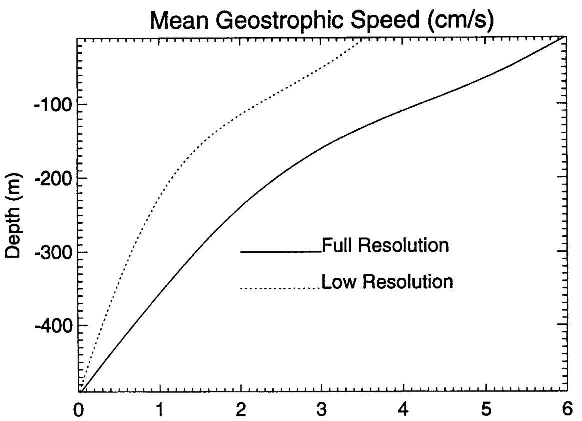

Fig. 13. Level-mean geostrophic speed referred to 500 m computed from the two data sets mentioned in Figs. 12a,b.

(and keeping the same estimate for U) would lead to a proportional increase of the Rossby number and, therefore, to a dubious application of the geostrophic assumption.

We therefore assume that the full resolution meso'95 data set can provide proper estimates of the geostrophic mesoscale circulation in the western basin of the Bransfield Strait. Conversely, the macro'95 and macro'96 data sets (those covering the whole domain) will only reflect the circulation associated with larger (>80 km) scales. In areas of mesoscale activity, geostrophic speeds computed from these data sets could underestimate actual speeds by as much as 40%, as suggested by Fig. 13.

References

Bryden, H.L., Pillsbury, R.D., 1977. Variability of deep flow in the Drake Passage from year-long current measurements. Journal of Physical Oceanography 7, 803–810.

Castro, C., Ríos, A., Doval, M.D., Perez, X., 2002. Spatio-temporal variability of nutrients utilization, chlorophyll distribution in the upper mixed layer during FRUELA 95 and FRUELA 96 cruises (Antarctica).

García, M.A., Castro, C.E., Ríos, A.F., Doval, M.D., Rosón, G., Gomis, D., López, O., 2002. Watermasses, distribution of physico-chemical properties in the Western Bransfield Strait and Gerlache Strait during Austral summer 1995/96. Deep-Sea Research II 49, 585–602.

Grelowski, A., Majewicz, A., Pastuszak, M., 1986. Mesoscale hydrodynamic processes in the region of the Bransfield Strait and the southern part of Drake Passage during BIOMASS-SIBEX 1983/84. Polish Polar Research 7, 353–369.

Holton, J.R., 1979. An Introduction to Dynamic Meteorology. International Geophysical Series, Vol. 23. Academic Press, New York.

Hoskins B, .J., Draghici, I., Davies, H.C., 1978. A new look at the omega equation. Quarterly Journal of the Royal Meteorological Society 104, 31–38.

Huntley, M., Karl, D.M., Niiler, P., Holm-Hansen, O., 1991. Research on Antarctic coastal ecosystem rates (RACER), an interdisciplinary field experiment. Deep-Sea Research I 38, 911–941.

López, O., García, M.A., Arcilla, A.S., 1994. Tidal and residual currents in the Bransfield Strait region, Antarctica. Annales Geophysicae 12 (9), 887–902.

López, O., García, M.A., Gomis, D., Rojas, P., Sospedra, J., Arcilla, A.S., 1999. Hydrographic and hydrodynamic characteristics of the eastern basin of the Bransfield Strait (Antarctica). Deep-Sea Research I 46, 1755–1778.

Niiler, P., Amos, A., Hu, J.-H., 1991. Water masses and 200 m relative geostrophic circulation in the western Bransfield Strait region. Deep-Sea Research I 38, 943–959.

Nowlin Jr., W.D., Zenk, W., 1988. Westward bottom currents along the margin of the South Shetland Island Arc. Deep-Sea Research I 35 (2), 269–301.

Nowlin Jr., W.D., Whitworth III, T., Pillsbury, R.D., 1977. Structure and transport of the Antarctic Circumpolar Current at Drake Passage from short-term measurements. Journal of Physical Oceanography 7, 788–802.

Orsi, A.H., Whitworth III, T., Nowlin Jr., W.D., 1995. On the meridional extent and fronts of the Antarctic Circumpolar Current. Deep-Sea Research I 42, 641–673.

Pedder, M.A., 1993. Interpolation and filtering of spatial observations using successive corrections and gaussian filters. Monthly Weather Review 117, 1675–1708.

Pedder, M.A., Gomis, D., 1998. Applications of EOF analysis to the spatial estimation of circulation features in the ocean sampled by high-resolution CTD soundings. Journal of Atmospheric and Ocean Technology 15, 959–978.

Pinot, J.M., Tintoré, J., Wang, D.P., 1996. A study of the omega equation for diagnosing vertical motions at ocean fronts. Journal of Marine Research 54, 239–259.

Whitworth III, T., Nowlin Jr., W.D., Worley, S.J., 1982. The net transport of the Antarctic Circumpolar Current through Drake Passage. Journal of Physical Oceanography 12, 960–971.